

# A Wide and Deep Exploration of Radio Galaxies with Subaru HSC (WERGS). III. Discovery of a $z = 4.72$ Radio Galaxy with the Lyman Break Technique

著者	Takuji Yamashita, Tohru Nagao, Hiroyuki Ikeda, Yoshiaki Toba, Masaru Kajisawa, Yoshiaki Ono, Masayuki Tanaka, Masayuki Akiyama, Yuichi Harikane, Kohei Ichikawa, Toshihiro Kawaguchi, Taiki Kawamuro, Kotaro Kohno, Chien Hsiu Lee, Kianhong Lee, Yoshiaki Matsuoka, Mana Niida, Kazuyuki Ogura, Masafusa Onoue, Hisakazu Uchiyama
journal or publication title	The Astronomical Journal
volume	160
number	2
page range	60
year	2020-07-09
URL	<a href="http://hdl.handle.net/10097/00130861">http://hdl.handle.net/10097/00130861</a>

doi: 10.3847/1538-3881/ab98fe



# A Wide and Deep Exploration of Radio Galaxies with Subaru HSC (WERGS). III. Discovery of a $z = 4.72$ Radio Galaxy with the Lyman Break Technique

Takuji Yamashita<sup>1,2</sup> , Tohru Nagao<sup>2</sup> , Hiroyuki Ikeda<sup>1,3</sup> , Yoshiki Toba<sup>2,4,5</sup> , Masaru Kajisawa<sup>2,6</sup> , Yoshiaki Ono<sup>7</sup>,  
Masayuki Tanaka<sup>1</sup> , Masayuki Akiyama<sup>8</sup> , Yuichi Harikane<sup>1</sup> , Kohei Ichikawa<sup>8,9</sup> , Toshihiro Kawaguchi<sup>10</sup>,  
Taiki Kawamuro<sup>1</sup> , Kotaro Kohno<sup>11,12</sup> , Chien-Hsiu Lee<sup>13</sup> , Kianhong Lee<sup>11</sup> , Yoshiki Matsuoka<sup>2</sup>, Mana Niida<sup>6</sup>,  
Kazuyuki Ogura<sup>14,15</sup>, Masafusa Onoue<sup>16</sup> , and Hisakazu Uchiyama<sup>1</sup>

<sup>1</sup> National Astronomical Observatory of Japan, 2-21-1 Osawa, Mitaka, Tokyo 181-8588, Japan; [takuji.yamashita@nao.ac.jp](mailto:takuji.yamashita@nao.ac.jp)

<sup>2</sup> Research Center for Space and Cosmic Evolution, Ehime University, 2-5 Bunkyo-cho, Matsuyama, Ehime 790-8577, Japan

<sup>3</sup> National Institute of Technology, Wakayama College, 77 Noshima, Nada, Gobo, Wakayama 644-0023, Japan

<sup>4</sup> Department of Astronomy, Kyoto University, Kitashirakawa-Oiwake-cho, Sakyo-ku, Kyoto 606-8502, Japan

<sup>5</sup> Academia Sinica Institute of Astronomy and Astrophysics, 11F of Astronomy-Mathematics Building, AS/NTU, No.1, Section 4, Roosevelt Road, Taipei 10617, Taiwan

<sup>6</sup> Graduate School of Science and Engineering, Ehime University, Bunkyo-cho, Matsuyama, Ehime 790-8577, Japan

<sup>7</sup> Institute for Cosmic Ray Research, The University of Tokyo, 5-1-5 Kashiwanoha, Kashiwa, Chiba 277-8582, Japan

<sup>8</sup> Astronomical Institute, Tohoku University, 6-3 Aramaki, Aoba-ku, Sendai, Miyagi 980-8578, Japan

<sup>9</sup> Frontier Research Institute for Interdisciplinary Sciences, Tohoku University, Sendai, Miyagi 980-8578, Japan

<sup>10</sup> Department of Economics, Management and Information Science, Onomichi City University, Onomichi, Hiroshima 722-8506, Japan

<sup>11</sup> Institute of Astronomy, School of Science, The University of Tokyo, 2-21-1 Osawa, Mitaka, Tokyo 181-0015, Japan

<sup>12</sup> Research Center for the Early Universe, The University of Tokyo, 7-3-1 Hongo, Bunkyo, Tokyo 113-0033, Japan

<sup>13</sup> NSF's National Optical-Infrared Astronomy Research Laboratory, 950 N. Cherry Ave., Tucson, AZ 85719, USA

<sup>14</sup> Faculty of Education, Bunkyo University, 3337, Minami-ogishima, Koshigaya, Saitama 343-8511, Japan

<sup>15</sup> Nishi-Harima Astronomical Observatory, Center for Astronomy, University of Hyogo, 407-2 Nishigaichi, Sayo, Hyogo 679-5313, Japan

<sup>16</sup> Max-Planck-Institut für Astronomie, Königstuhl 17, D-69117 Heidelberg, Germany

Received 2019 November 14; revised 2020 May 24; accepted 2020 June 1; published 2020 July 9

## Abstract

We report a discovery of a  $z = 4.72$  radio galaxy, HSC J083913.17+011308.1, using the Lyman break technique with the Hyper Suprime-Cam Subaru Strategic Survey (HSC-SSP) catalog for Very Large Array Faint Images of the Radio Sky at Twenty centimeter radio sources. The number of known high- $z$  radio galaxies (HzRGs) at  $z > 3$  is quite small to constrain the evolution of HzRGs so far. The deep and wide-area optical survey by HSC-SSP enables us to apply the Lyman break technique to a large search for HzRGs. For an HzRG candidate among pre-selected  $r$ -band dropouts with a radio detection, a follow-up optical spectroscopy with the Gemini Multi-Object Spectrographs (GMOS)/Gemini has been performed. The obtained spectrum presents a clear Ly $\alpha$  emission line redshifted to  $z = 4.72$ . The spectral energy distribution fitting analysis with the rest-frame UV and optical photometries suggests the massive nature of this HzRG with  $\log M_*/M_\odot = 11.4$ . The small equivalent width of Ly $\alpha$  and the moderately red UV colors indicate its dusty host galaxy, implying a chemically evolved and dusty system. The radio spectral index does not meet a criterion for an ultra-steep spectrum,  $\alpha_{1400}^{325}$  of  $-1.1$  and  $\alpha_{1400}^{150}$  of  $-0.9$ , demonstrating that the HSC-SSP survey compensates for a subpopulation of HzRGs that are missed in surveys focusing on an ultra-steep spectral index.

*Unified Astronomy Thesaurus concepts:* [Radio galaxies \(1343\)](#); [Active galaxies \(17\)](#); [High-redshift galaxies \(734\)](#); [Lyman-break galaxies \(979\)](#); [Spectroscopy \(1558\)](#)

## 1. Introduction

Observations and numerical studies suggest that feedback effects from radio galaxies (RGs) can play a key role on the evolution of galaxies by regulating star formation (e.g., McNamara et al. 2005; Croton et al. 2006; Wagner & Bicknell 2011; Fabian 2012; Morganti et al. 2013). It is important to describe the number densities of RGs along the cosmic time up to the early universe for understanding the evolution of galaxies and active galactic nuclei (AGNs). In particular, high- $z$  RGs (HzRGs) at  $z > 2$  represent a key population to reveal the formation of massive galaxies and massive galaxy clusters (Miley & De Breuck 2008), because the stellar mass of HzRGs is typically as massive as  $>10^{11} M_\odot$  even at  $z > 3$  (Seymour et al. 2007; De Breuck et al. 2010) and the gas metallicity of HzRGs at  $z > 3$  exceeds the solar metallicity (Nagao et al. 2006; Matsuoka et al. 2009). The most massive galaxies could be rapidly formed before  $z \sim 3$  (e.g., Pérez-González et al. 2008). The number density of RGs moderately increases up to  $z \sim 1-2$  and is

believed to abruptly decline at the HzRG regime at  $z = 2-3$  (Dunlop & Peacock 1990; Rigby et al. 2015). At  $z > 3$ , the number density of HzRGs is not well constrained due to a dearth of samples, except a small number of known radio-loud quasars (Bañados et al. 2015).

HzRGs have been historically discovered using a radio spectral index. HzRGs are empirically known to show an ultra-steep spectrum (USS), which is commonly defined as a spectrum with a radio spectral index  $\alpha$  of  $< -1.3$  (De Breuck et al. 2000b; Saxena et al. 2018a, 2019). The USS selection is based on an idea of a steepening radio spectrum with frequency and redshifting (e.g., Carilli & Yun 1999; Morabito & Harwood 2018). The technique using USS was successfully established and is an efficient method to find a lot of HzRGs (De Breuck et al. 2000b). The  $z = 5.19$  HzRG, TN J0924-2201, had been discovered with the USS technique and had been the most distant known HzRG record in the past two decades (van Breugel et al. 1999). Recently, Saxena et al. (2018b) broke the redshift record and discovered a  $z = 5.72$  HzRG, TGSS J1530+1049, using the USS technique.

However, a small number of  $z > 4$  HzRGs without USS has been discovered: non-USS HzRGs at  $z = 4.42$  (VLA J123642+621331; Waddington et al. 1999) and  $z = 4.88$  (J163912.11+405236.5; Jarvis et al. 2009) were discovered out of radio-detected but very faint objects in optical and near-infrared, respectively. The spectral indices of these two HzRGs are  $-0.94$  between 1.4 GHz and 8.5 GHz and  $-0.75$  between 325 MHz and 1.4 GHz, respectively. Their radio morphologies are compact and must be associated with an AGN. Klamer et al. (2006) indicated that no HzRGs selected based on USS show a curvature in gigahertz spectra. These facts suggest the known HzRGs are a tip of the iceberg. Therefore the true spectral index distribution in HzRGs is unclear. The present biased sample of HzRGs toward USS could lead to misunderstandings of the number density of HzRGs and underlying radio luminosity functions (Jarvis & Rawlings 2000; Jarvis et al. 2001; Yuan et al. 2016, 2017).

Finding HzRGs without relying on the USS technique is now possible using the Lyman break technique on deep optical imaging (e.g., Steidel et al. 1996). Great advances of instruments capable deep imaging surveys in wide fields enable us to identify very faint and rare objects such as HzRGs. A search for HzRGs using the Lyman break technique will provide a uniform HzRG sample without biases of radio spectral indices. The Hyper Suprime-Cam Subaru Strategic Survey (HSC-SSP; Aihara et al. 2018a; Furusawa et al. 2018; Kawanomoto et al. 2018; Komiyama et al. 2018; Miyazaki et al. 2018) is one of the most suitable programs for this purpose. The Lyman break technique for HSC-SSP photometric objects was successfully applied to search for high- $z$  galaxies (Harikane et al. 2018; Ono et al. 2018; Toshikawa et al. 2018) and high- $z$  quasars (e.g., Matsuoka et al. 2016, 2018a, 2018b, 2019; Akiyama et al. 2018). In this paper, we report a discovery of  $z = 4.7$  HzRG, HSC J083913.17+011308.1 (hereafter HSC J0839+0113), found out of a pilot survey sample using Subaru HSC and an archival radio catalog. This survey is part of an ongoing project, a Wide and Deep Exploration of RGs with Subaru HSC (WERGS; Yamashita et al. 2018). This paper is the third in a publication series of WERGS, which follows Yamashita et al. (2018) and Toba et al. (2019) and precedes Ichikawa et al. (2020, submitted). Throughout this paper, all magnitudes are presented in the AB system (Oke & Gunn 1983) and are corrected for Galactic extinction (Schlegel et al. 1998). We use the CModel photometry for HSC data (Abazajian et al. 2004). We use a flat  $\Lambda$ CDM cosmological model with  $H_0 = 70 \text{ km s}^{-1} \text{ Mpc}^{-1}$  and  $\Omega_M = 0.30$ . Using this cosmology, at  $z = 4.7$  the age of the universe is 1.2 Gyr and  $1''$  corresponds to 6.5 kpc.

## 2. Selection

We utilized the 1.4 GHz radio continuum catalog of the Faint Images of the Radio Sky at Twenty-centimeters survey (FIRST; Becker et al. 1995) with Very Large Array (VLA). FIRST surveyed the area of the Sloan Digital Sky Survey (York et al. 2000) and thus entirely covers the HSC-SSP survey fields with a spatial resolution of  $5''4$ . We only used radio sources with a peak flux of greater than 1 mJy and a side lobe probability<sup>17</sup> of less than 0.05 in the final release catalog (Helfand et al. 2015).

In order to identify optical counterparts of FIRST sources, we used a forced photometry catalog in the wide layer of the

internally released version, S16A Wide2, of HSC-SSP (Aihara et al. 2018b). The forced photometries were performed for each image using position and shape parameters determined in a reference band. The order of the priority bands as a reference band is *irzyg* according to its signal-to-noise ratio (S/N) approximately (see Bosch et al. 2018, for more details). Only a unique object that has been deblended and photometric based on the *i* band was selected by flags, `detect_is_primary` and `merge_measurement_i`, in the HSC-SSP database. Further, we imposed the following criteria on objects: in the *i*, *r*, and *z* bands, an object is not affected by cosmic rays (`flags_pixel_cr_center`), not saturated (`flags_pixel_saturated_center`), and not at the edge of a CCD or a coadded image (`flags_pixel_edge` for removing); in the *i* and *z* bands, there are no problems in the photometries (`cmodel_flux_flags`, `centroid_sdss_flags`); the number of visits at an object position (`countinputs`) is greater than or equal to 4 (6) for the *g* and *r* (*i* and *z*) bands to ensure a certain observing depth. We have cross-matched between the FIRST sources and the HSC-SSP sources with a search radius of  $1''$ . This search radius was set to balance between contamination and completeness, where the estimated contamination by chance coincidence is 14% (see Yamashita et al. 2018 for the details).

Out of 4725 matched sources, 16 sources were selected as *r*-dropouts with  $S/N > 5$  in the *z* band, which meet the following color criteria, which are the same ones as those of Ono et al. (2018),

$$r_{AB} - i_{AB} > 1.2 \quad (1)$$

$$i_{AB} - z_{AB} < 0.7 \quad (2)$$

$$r_{AB} - i_{AB} > 1.5(i_{AB} - z_{AB}) + 1.0. \quad (3)$$

The objects further should be not detected in the *g* band or  $g_{AB} > r_{AB}$ . These *r*-dropouts are candidates of HzRGs at  $z \sim 5$  (Figure 1). HSC J0839+0113 was selected out of them according to the brightness ( $z_{AB} < 25$ ) and the visibility for a follow-up observation with the Gemini Multi-Object Spectrographs (GMOS)/Gemini (see the next section). HSC J0839+0113 has a FIRST 1.4 GHz flux of  $7.17 \pm 0.14 \text{ mJy}$  (see also Table 1). Its HSC images and FIRST radio continuum are displayed in Figure 2. The obvious dropout at the *r* band is seen. The apparent size in the FIRST image is approximately a point source ( $\text{FWHM} = 6''25 \times 5''30$ ), as seen in high- $z$  radio sources. There are no other HSC sources within the FIRST beam.

## 3. Spectroscopic Redshift and Photometric Data

### 3.1. Spectroscopic Follow-up Observation

A long-slit spectroscopy was performed for HSC J0839+0113 using GMOS mounted on the Gemini South telescope on 2018 February 21 (Program ID: GS-2017B-FT-17; PI: T. Yamashita) in order to obtain its spectroscopic redshift. We used the OG515 filter and the R400-G5305 grating blazed at 8300 Å. The slit width was set to be  $1''0$ . The spectral resolution is approximately 8 Å, which corresponds to  $290 \text{ km s}^{-1}$ . The spectral coverage was typically 6700–10000 Å. The position angle was set to be  $32^\circ56'$  east of north. A total of  $7 \times 1030 \text{ s}$  exposures were obtained. Bias frames, flat-fields, CuAr arcs, and standard star Hiltner 600 were also taken for calibration. The seeing of the observation was  $0''99$ .

<sup>17</sup> The side lobe probability is a measure of a likelihood that a source is a spurious detection near a bright source.

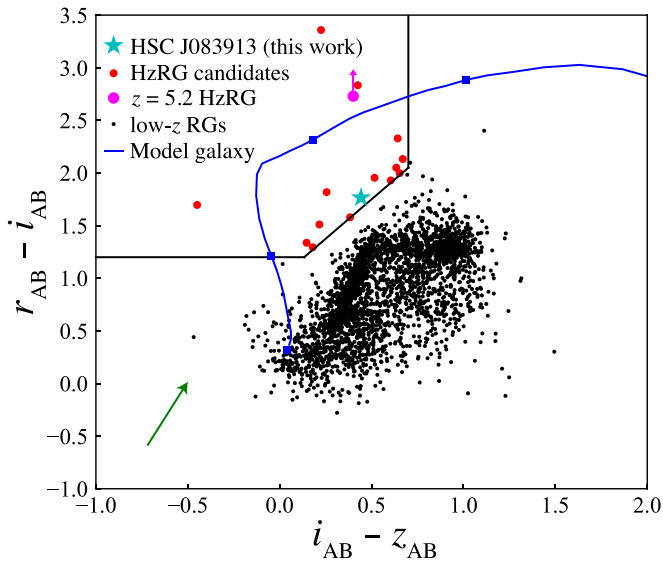


**Figure 1.** Color-color diagram for selecting HzRG candidates at  $z \sim 5$ . The candidates are denoted by the red circles and are inside the color selection criteria (black lines; Ono et al. 2018). One candidate is out of the  $y$ -axis range. The cyan star represents HSC J0839+0113. The magenta circle denotes the colors of the known HzRG at  $z = 5.2$ , where the filters used were slightly different from those of HSC and the  $y$ -axis is a lower limit (Overzier et al. 2006). The blue line indicates the color track of a star-forming galaxy model produced with a stellar synthesis code of Bruzual & Charlot (2003). The model assumes an instantaneous-burst model with an age of 25 Myr, the solar metallicity, the intergalactic medium absorption of Madau (1995), and Lyman $\alpha$  emission with a rest-frame equivalent width of 1180 Å and an observed frame FWHM of 1530 km s $^{-1}$  (the most large equivalent width case in  $z > 2$  HzRGs of Roettgering et al. 1997). The squares on the track mark redshifts of 4.0, 4.5, 5.0, and 5.5. The black dots show low- $z$  RGs in the WERGS sample (Yamashita et al. 2018). The green vector shows the extinction vector of  $A_V = 1$  (Calzetti et al. 2000).

Data reduction was carried out using the Gemini/GMOS IRAF package. Object frames were bias-subtracted and flat-fielded. The wavelength calibration for the object frames was performed using reduced arc frames. After removing cosmic rays, subtracting sky lines, and flux calibration using the spectrophotometric standard star (Hiltner 600), the object frames were combined with median stacking. A 1D spectrum was extracted with an aperture of 1".9.

The Ly $\alpha$   $\lambda$ 1216 emission line is significantly detected at a peak of 6957 Å in the spectrum (Figure 3). The redshifted Ly $\alpha$  corresponds to a redshift of  $4.723 \pm 0.001$ . The characteristic asymmetric profile of this emission line (see the right panel of Figure 3) and the  $r$ -dropout of this object credibly support that this line is the redshifted Ly $\alpha$ , although any other lines were not identified in this spectrum. Continuum is also detected at a part redder than the Ly $\alpha$  line while it is not detected in the bluer part, which is consistent with Ly $\alpha$  break at this redshift. The 2D spectrum shows an extended Ly $\alpha$  of 1".3, which corresponds to 8.4 kpc. This extended Ly $\alpha$  is approximately equivalent to a deconvolved size of 7.6 kpc in the 1.4 GHz image produced by the FIRST survey project (Helfand et al. 2015).

### 3.2. Spectral Energy Distribution Fitting Analysis

We estimate a stellar mass of this HzRG by a fitting analysis of its spectral energy distribution (SED). Photometric data of the VISTA Kilo-degree Infrared Galaxy Survey (VIKING; Edge et al. 2013) and ALLWISE (Cutri et al. 2014) are

**Table 1**  
Properties of HSC J083913.17+011308.1

R.A., decl. (J2000)	08 <sup>h</sup> 39 <sup>m</sup> 13 <sup>s</sup> .17, +01 <sup>o</sup> 13 <sup>m</sup> 08 <sup>s</sup> .1
Redshift	4.723 (0.001)
$r_{AB}, i_{AB}$	25.66 (0.18), 23.89 (0.03)
$z_{AB}, y_{AB}$	23.45 (0.04), 23.23 (0.06)
$Z_{AB}, Y_{AB}, J_{AB}$	23.81 (0.03), 23.1 (0.4), 22.6 (0.5)
$H_{AB}, Ks_{AB}$	>22.4 <sup>a</sup> , 22.4 (0.5)
FIRST $S_{1.4\text{GHz}}$	7.17 (0.14) mJy
GMRT $S_{325\text{MHz}}$	36.8 (2.0) mJy
TGSS $S_{150\text{MHz}}$	54.5 (6.6) mJy
$L_{1.4\text{GHz}}$	1.63 (0.03) $\times 10^{27}$ W Hz $^{-1}$
$L_{325\text{MHz}}$	8.38 (0.46) $\times 10^{27}$ W Hz $^{-1}$
$L_{150\text{MHz}}$	12.4 (1.5) $\times 10^{27}$ W Hz $^{-1}$
$\alpha_{325}^{1400}$	-1.12 (0.02)
$\alpha_{150}^{1400}$	-0.91 (0.02)
Ly $\alpha$ flux	4.3 (0.4) $\times 10^{-17}$ erg s $^{-1}$ cm $^{-2}$
Ly $\alpha$ luminosity	9.80 (0.10) $\times 10^{42}$ erg s $^{-1}$
Ly $\alpha$ FWHM	660 (90) km s $^{-1}$
Ly $\alpha$ EW $_{\text{rest}}$	9.1 (1.6) Å
log $M_*/M_{\odot}$ <sup>b</sup>	11.43 ( $^{+0.22}_{-0.46}$ )

**Notes.** 1 $\sigma$  errors are shown in parentheses.

<sup>a</sup> 3 $\sigma$  upper limit.

<sup>b</sup> The stellar mass is derived from the spectral energy distribution fitting.

available for this object, as well as HSC-SSP (see Figure 2 for images of all bands). Because no entry of this object is in the VIKING DR3 source catalog likely due to its low S/N, we performed aperture photometries on archive VIKING images of all ZYJHKs bands. The VIKING images are convolved to match their point-spread function (PSF) to one of the Z band, after sky backgrounds are subtracted. The 2".5 aperture is used for the object photometries. This aperture radius at the object position encloses an equivalent flux of a  $i$ -band image convolved to the Z band to the CModel  $i$ -band flux. Therefore the 2".5 aperture photometries can measure a total flux of the object. The errors in the photometries are estimated from variations of aperture photometries at object-free regions. Only in the J band, two archive image frames are available for this object. We note that two photometry results of these frames are significantly different from each other. This large difference is likely due to an effect from large-scale variations of sky backgrounds on the low S/N images. Thus, we use a weighted mean of the two photometries for the SED fitting analysis. Finally, we obtain 23.81 (0.03), 23.1 (0.4), 22.6 (0.5), >22.4, and 22.4 (0.5) in the ZYJHKs bands, respectively. The parentheses represent 1 $\sigma$  errors. For a nondetection in the H band, the 3 $\sigma$  limit is provided. In ALLWISE, there are no entries in the catalog of both bands of W1 and W2. Even in the images, the object is not detected in both bands, after a possible contamination from an adjacent object is considered (a source at the southeast from HSC J0839+0113 in Figure 2). We thus put 3 $\sigma$  upper limits of 32  $\mu$ Jy and 43  $\mu$ Jy for W1 and W2, respectively.

SED fitting is performed with these optical-to-mid-infrared photometries including upper limits using the Code Investigating GALaxy Emission (CIGALE) SED fitting code (Burgarella et al. 2005; Boquien et al. 2019). We basically follow an SED fitting manner of Toba et al. (2019), who applied the CIGALE SED fitting for HSC-selected RGs, but we use somewhat smaller steps of free parameters than Toba et al. (2019) and do

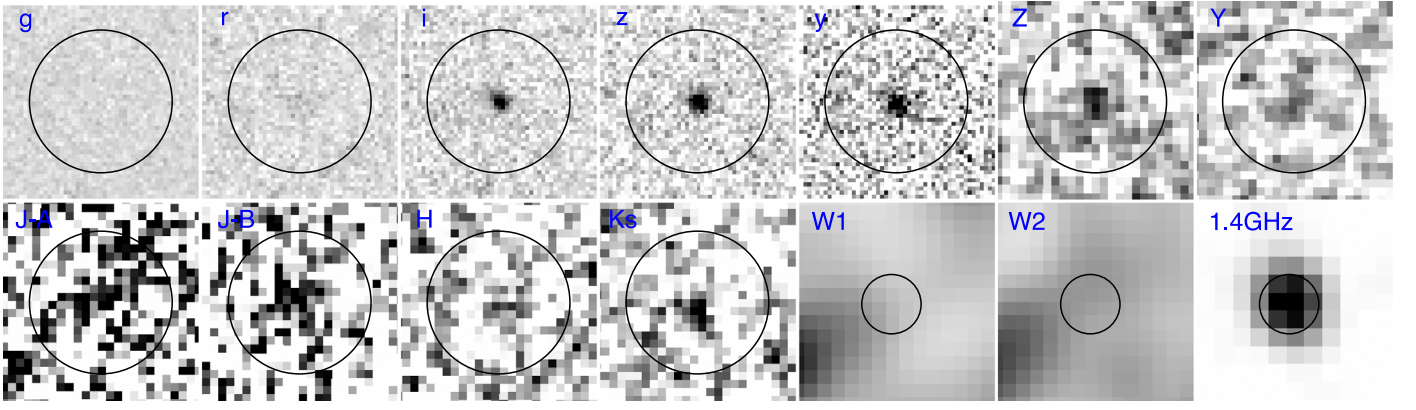


**Figure 2.** Postage stamp images of HSC J0839+0113. From top left to bottom right, the Subaru HSC *grizy* and VIKING *ZYJKs* images are shown with a width of  $8''$ , and subsequently the Wide-field Infrared Survey Explorer (WISE) W1W2 and FIRST 1.4 GHz images with a width of  $20''$ . Two frames of the VIKING *J* band, denoted by *J-A* and *J-B*, respectively, are shown and the results of the spectral energy distribution fitting with each *J*-band photometries are discussed in Section 4.2. North is upward and east is to the left. There are no other optical/near-infrared sources within the FIRST detection region (FWHM  $\sim 6''$ ). The infrared counterparts in both W1 and W2 are not detected. Circles with an equivalent diameter of  $6''$  to the apparent size in the FIRST image serve as a guide to the eye.

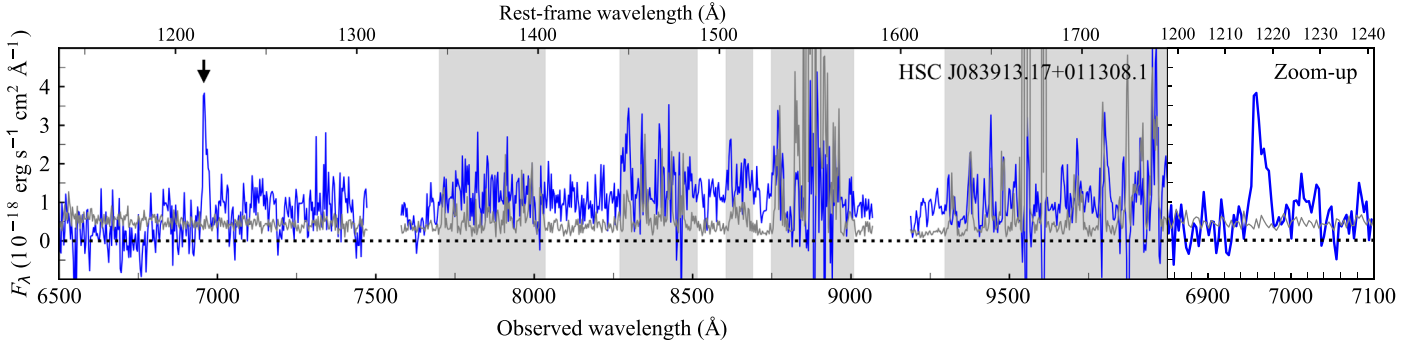


**Figure 3.** GMOS spectrum of HSC J0839+0113. The redshifted Ly $\alpha$  to  $z = 4.723$  is shown at  $6957 \text{ \AA}$  in the observed frame (black arrow). The Ly $\alpha$  break is also detected at a part bluer than the Ly $\alpha$  line. The full spectrum (blue thin line) and the enlarged spectrum around the Ly $\alpha$  emission line (blue thick line) are shown. A noise spectrum (gray line) serves as a guide to the expected noise. The wavelength regimes strongly affected by sky lines are shaded. The missing data points are due to CCD gaps.

not include models of infrared dust emission, radio synchrotron emission, and AGN emission. In our SED fitting analysis, the star formation history of two exponential decreasing star formations with different  $e$ -folding times is assumed. A stellar template of Bruzual & Charlot (2003) with an initial mass function of Chabrier (2003) is adopted. Dust attenuation is modeled by the dust extinction law of Calzetti et al. (2000). The SED fitting with CIGALE also handle fluxes with upper limits by introducing the error functions for computing  $\chi^2$  (see Boquien et al. 2019).

The best-fit SED model is presented in Figure 4. The reduced  $\chi^2$  of the best fit is 0.46 with a degree of freedom of 10. The bayesian-estimated stellar mass is  $\log M_*/M_\odot = 11.43^{+0.22}_{-0.46}$ , where the super/subscripts are  $1\sigma$  errors. The mass-weighted age is 230 (160) Myr. We cross-checked the stellar mass with that estimated with the Mizuki SED template-fitting code (Tanaka 2015), where the Mizuki fitting was performed for all the photometry data of this object. The estimated stellar mass is  $11.66^{+0.24}_{-0.26}$ . The Mizuki result is consistent with that of CIGALE within the  $1\sigma$  errors. We do not provide the star formation rate (SFR) from this SED fitting analysis because the SFR is not constrained due to the lesser number of photometry data in the observed frame infrared wavelength. The results are further discussed in Section 4.2.

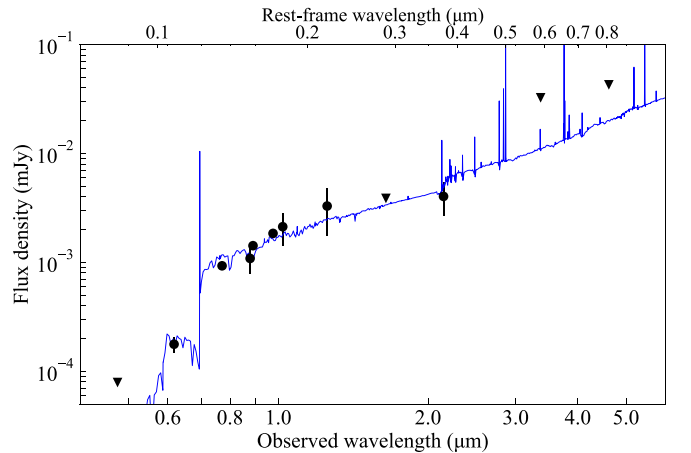


**Figure 4.** SED of HSC J0839+0113 and its best-fit models. The plotted data are photometries of *grizy* (HSC), *ZYJKs* (VIKING), and W1W2 (WISE). The circles and triangles denote detections with  $1\sigma$  error bars and nondetection ( $3\sigma$  upper limits), respectively.

## 4. Discussion: The Nature of HSC J0839+0113

### 4.1. Radio Properties

HSC J0839+0113 was selected from Lyman break galaxies (LBGs) with a radio detection of FIRST. Because any criteria

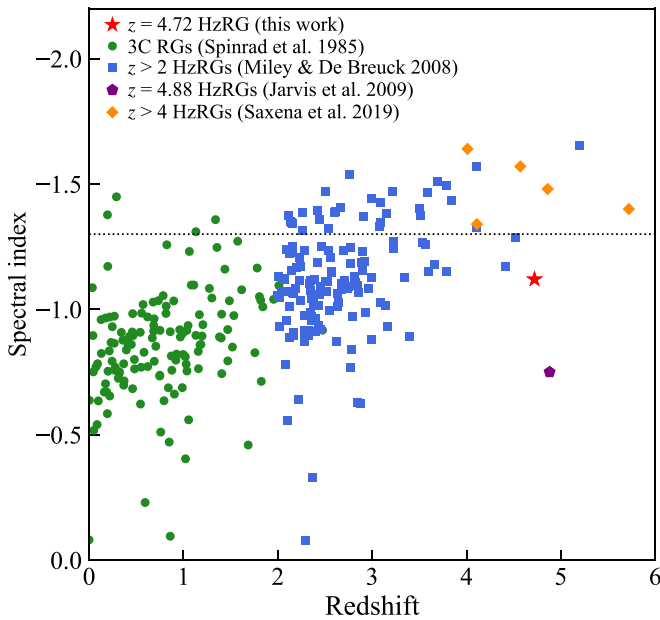


**Figure 5.** Radio spectral index ( $\alpha$ ;  $S_\nu \propto \nu^\alpha$ ) as a function of redshift of RGs. The red star indicates the HSC J0839+0113 in this paper. The known RGs taken from literature are also plotted: 3CR (green circles; Spinrad et al. 1985), the HzRG sample at  $z > 2$  (blue squares; Miley & De Breuck 2008), the  $z = 4.88$  non-USS HzRG (purple pentagon; Jarvis et al. 2009), and the five recently discovered HzRGs at  $z > 4$  (orange diamonds; Saxena et al. 2019). The commonly used criterion of  $\alpha$  for USS selection is represented by a dotted line.

on a radio spectral index are not imposed to the selection, discussing its radio properties is relevant. Radio photometric data of HSC J0839+0113 are available in the FIRST 1.4 GHz catalog (Helfand et al. 2015), the 325 MHz Giant Metrewave Radio Telescope (GMRT) survey catalog in the Herschel-ATLAS/ Galaxy And Mass Assembly (GAMA) field (Mauch et al. 2013), and the 150 MHz TIFR GMRT Sky Survey (TGSS) Alternative Data Release (Intema et al. 2017).

The spectral indices  $\alpha$  ( $S_\nu \propto \nu^\alpha$ ) are calculated to be  $\alpha_{1400}^{150} = -0.91$  (0.02) between 150 MHz and 1.4 GHz, and  $\alpha_{1400}^{325} = -1.12$  (0.02) between 325 MHz and 1.4 GHz, respectively. Alternative spectral index of  $\alpha_{1400}^{150}$  is  $-0.84$  in the spectral index catalog by de Gasperin et al. (2018) who reprocessed the TGSS and the NRAO VLA Sky Survey (NVSS) images. These indices do not meet the criterion defining ultra-steep spectral index,  $\alpha < -1.3$  (De Breuck et al. 2000b; Saxena et al. 2018a).

In Figure 5, the spectral index between 325 MHz and 1.4 GHz is shown as a function of redshift together with other known HzRGs. The spectral indices of the other RGs and HzRGs are taken from literature: 3CR (Spinrad et al. 1985), the HzRG sample at  $z > 2$  (Miley & De Breuck 2008), the  $z = 4.88$  non-USS HzRG with  $\alpha = -0.75$  (Jarvis et al. 2009), and the five recently discovered HzRGs at  $z > 4$  ( $\alpha$  of from  $-1.34$  to  $-1.64$ ; Saxena et al. 2019). The spectral indices of the literature samples are calculated between WENSS 325 MHz (Rengelink et al. 1997) and NVSS 1.4 GHz (Condon et al. 1998) or between TEXAS 365 MHz (Douglas et al. 1996) and NVSS 1.4 GHz except for Saxena’s HzRGs. The spectral indices for  $z > 4$  Saxena’s HzRGs are calculated between VLA 370 MHz and 1.4 GHz (Saxena et al. 2018a) except for the most distant known HzRG at  $z = 5.72$  (TGSS J1530+1049) with a spectral index of  $-1.4$  between TGSS 150 MHz and

VLA 1.4 GHz (Saxena et al. 2018b). We can see the  $\alpha - z$  correlation at all of the redshift range. At  $z > 4$ ,  $z = 4.88$  HzRG (J163912.11+405236.5) shows the flattest spectral index. This object has been discovered out of faint mid-infrared sources with a FIRST detection in the Spitzer Wide-Area Infrared Extragalactic Survey deep field, not by using the USS technique (Jarvis et al. 2009). This is an evident example illustrating non-USS HzRGs at  $z > 4$ . VLA J1236421+621331, another non-USS HzRG at  $z = 4.42$  (Waddington et al. 1999), is not plotted here because the low-frequency photometry data is not available. HSC J0839+0113 is located below the  $\alpha = -1.3$  selection line (the dotted line in Figure 5), following the  $z = 4.88$  HzRG at  $z > 4$ . HSC J0839+0113 would be never discovered using the USS technique. This discovery of the non-USS HzRG at  $z \sim 5$ , along with the previously reported non-USS HzRGs at  $z \sim 4-5$  (Waddington et al. 1999; Jarvis et al. 2009), suggests that a subset of HzRGs is missed in many USS-based surveys.

The rest-frame radio luminosities of HSC J0839+0113 are  $\log L_{1.4 \text{ GHz}} = 27.2 \text{ W Hz}^{-1}$  and  $\log L_{150 \text{ MHz}} = 28.1 \text{ W Hz}^{-1}$ , assuming a mean spectral index,  $\alpha = -1.0$ , between  $\alpha_{1400}^{325}$  and  $\alpha_{1400}^{150}$ . Owing to the relatively flat spectrum, the radio luminosities at low frequency is one order of magnitude smaller than those of the previously reported USS-selected HzRGs at  $z \sim 4-5$ , and is a factor of 2–4 smaller than those of the recently reported USS-selected HzRGs at  $z \sim 4-5$  (Saxena et al. 2019).

#### 4.2. Host Galaxy

HzRGs are often involved with massive hosts ( $> 10^{11} M_\odot$ ; Seymour et al. 2007; De Breuck et al. 2010). We can examine whether HSC J0839+0113, which was selected among LBGs, follows the trend or not using the SED fitting result. The obtained stellar mass of HSC J0839+0113 is  $\log M_*/M_\odot = 11.4$  and is as massive as other known HzRGs (Seymour et al. 2007; De Breuck et al. 2010). This massive stellar mass of the host galaxy is supported from the fact that the apparent  $K_s$  magnitude of 20.6 Vega mag well follows the  $K - z$  correlation for HzRGs, where the correlation is established because of the characteristic massive stellar mass of known HzRGs (e.g., Rocca-Volmerange et al. 2004). HSC J0839+0113, which is an LBG with a radio-AGN, is one of the most massive galaxies among  $z \sim 5$  LBGs, which typically have  $\log M_*/M_\odot = 8 - 11$  (Yabe et al. 2009). Such a large stellar mass at  $z = 4.72$  (at an age of the universe of 1.2 Gyr) suggests that the stellar mass had been rapidly built up through intense star formation. Since HSC J0839+0113 is already very massive at the observed redshift, the star formation should either have been quenched by now or be quenched shortly, and then this HzRG could evolve into a giant elliptical galaxy seen at the present day.

#### 4.3. Ly $\alpha$ Emission

The measured Ly $\alpha$  line flux and luminosity of HSC J0839+0113 are  $4.3 \times 10^{-17} \text{ erg s}^{-1} \text{ cm}^{-2}$  and  $9.8 \times 10^{42} \text{ erg s}^{-1}$ , respectively. The underlying continuum is estimated from the continuum of 7000–7300 Å in the spectrum, assuming a flat continuum. Ly $\alpha$  emission is not corrected for extinction. The Ly $\alpha$  luminosity is consistent with those of other  $z \sim 4-5$  HzRGs (van Breugel et al. 1999; Kopylov et al. 2006; Jarvis et al. 2009; Saxena et al. 2019). The Ly $\alpha$  FWHM is derived with a single

Gaussian fitting and is corrected for the instrumental broadening effect. The derived FWHM is  $660 \text{ km s}^{-1}$ . The FWHM is smaller than those of the known HzRGs at  $z > 2$ , which have typically  $>1000 \text{ km s}^{-1}$ . This narrow FWHM of Ly $\alpha$  could suggest that a dominant ionization source of Ly $\alpha$  of HSC J0839+0113 is neither a broad emission line AGN nor jet-induced shock, but rather star formation or a weak AGN. Saxena et al. (2019) argue that the dominant source of faint HzRGs with low Ly $\alpha$  luminosities ( $\sim 10^{43} \text{ erg s}^{-1}$ ) and narrow FWHMs ( $<600 \text{ km s}^{-1}$ ) at  $z > 4$  could be star formation or a weak AGN compared with Ly $\alpha$  emitters. Our result is not inconsistent with that.

Equivalent width  $EW_{\text{rest}}$  of Ly $\alpha$  at the rest-frame is calculated to be  $9 (1.6) \text{ \AA}$  from the obtained spectrum. The  $EW_{\text{rest}}$  of HSC J0839+0113 is much smaller than those of the known HzRGs. The known HzRGs at  $2 < z < 4$  show large  $EW_{\text{rest}}$  of up to  $\sim 700 \text{ \AA}$ . For almost all of the HzRGs at  $z > 4$ , continua are not detected and the upper limits of  $EW_{\text{rest}}$  are measured to be  $>40\text{--}180 \text{ \AA}$  (Waddington et al. 1999; De Breuck et al. 2000a; Saxena et al. 2018b). The small  $EW_{\text{rest}}$  of HSC J0839+0113 is probably due to a mixture of its ionization source and optical brightness. UV emission lines of HzRGs are generally explained by photoionization by a powerful AGN and additionally jet-induced shock (e.g., De Breuck et al. 2000a). As discussed above, however, in HSC J0839+0113 the contributions from a powerful AGN or shock must be insignificant. The different ionization source in HSC J0839+0113, therefore, could result in the weak Ly $\alpha$  emission. In addition to the ionization source, the relative bright optical continuum of HSC J0839+0113 ( $z_{\text{AB}} = 23.5$ ) also likely causes the small  $EW_{\text{rest}}$ . The rest-frame UV continuum emission of HSC J0839+0113 is detected both in HSC and the Gemini spectroscopy, while  $z > 4$  HzRGs are not detected ( $>23 \text{ mag}$ ).

A small  $EW_{\text{rest}}$  is observed as the Ly $\alpha$  deficiency in luminous LBGs (Ando et al. 2006) and is attributed to a dusty absorption in a star-forming galaxy. The obtained small  $EW_{\text{rest}}$  and the relatively optical brightness indicate its dusty system associated with HSC J0839+0113. This is consistent with the migration on the *riz* diagram in Figure 1 from the model colors of a  $z \sim 4.7$  LBG to redder colors which suggests this dusty system. The colors of HSC J0839+0113 cannot be explained by galaxy models with low metallicity, although a low-metallicity galaxy at  $z \sim 5.2$  could have a similar color to that of HSC J0839+0113. These results support the abundant dust contents in HSC J0839+0113 and suggest the chemically evolved host. Submillimeter continua are detected in approximately half of HzRGs at  $2.5 < z < 4$  (Reuland et al. 2004), indicating the presence of dust. Only two  $z > 4$  HzRGs (TN J1338-1942 at  $z = 4.11$  and TN J0924-2201 at  $z = 5.19$ ) were observed with (sub)millimeter telescopes and their continua were detected (De Breuck et al. 2004; Falkendal et al. 2019). Although these two cases suggest the presence of cold dust there despite their large Ly $\alpha$   $EW_{\text{rest}}$  of  $200 \text{ \AA}$  and  $>180 \text{ \AA}$ , respectively, their Ly $\alpha$  emission are likely powered by a broad emission line AGN or jet-induced shock because of their large Ly $\alpha$  velocity widths of  $1000$  and  $1500 \text{ km s}^{-1}$ .

## 5. Summary

This paper reports the discovery of HSC J0839+0113, a  $z = 4.72$  HzRG, in the ongoing program to search for HzRGs as part of the WERGS project. HSC J0839+0113 was selected

as a HzRG candidate from the HSC data using the Lyman break technique. The redshift was determined with the Ly $\alpha$  emission line in the obtained Gemini/GMOS spectrum. From the analyses of the GMOS spectrum and photometric data, we found the following.

1. By the SED fitting with the rest-frame UV–optical photometries, the massive stellar mass of the host galaxy was estimated to be  $\log M_*/M_\odot = 11.4$  and is consistent with other known HzRGs but marks one of the most massive galaxies among LBGs at  $z = 5$ .
2. The Ly $\alpha$  line luminosity and FWHM are similar to those of other known  $z \sim 4\text{--}5$  HzRGs. The small  $EW_{\text{rest}}$  of HSC J0839+0113 is much different from HzRGs at  $2 < z < 4$  but consistent with the Ly $\alpha$  deficiency in luminous LBGs, suggesting a dusty host galaxy of HSC J0839+0113. The rest-frame UV colors seen on the *riz* color–color diagram are redder than those of the  $z \sim 5$  LBG model and also support the dusty and chemically evolved host galaxy.
3. HSC J0839+0113 has the relatively flat radio spectral index  $\alpha_{1400}^{325}$  of  $-1.1$  and thus does not belong to USS HzRGs.

The discovery of HSC J0839+0113 demonstrates the ability of HSC-SSP to find HzRGs without a radio spectral index. A HzRG sample established based on HSC-SSP compensates for a subpopulation of HzRGs that are missed in USS selection surveys. Because the HzRG was found out of the pilot selection sample in the early release data of HSC-SSP, the full data set of HSC-SSP covering  $1400 \text{ deg}^2$  has a potential for finding much more HzRGs at  $z > 3$ , at which known HzRGs are poor in numbers. HzRGs in our survey will provide new knowledge on the formation and evolution of massive galaxies and radio-AGNs at the early universe.

We thank the anonymous referee for the comments that improved this paper. We would like to thank Hiroshi Nagai for useful discussions.

The Hyper Suprime-Cam (HSC) collaboration includes the astronomical communities of Japan and Taiwan, and Princeton University. The HSC instrumentation and software were developed by the National Astronomical Observatory of Japan (NAOJ), the Kavli Institute for the Physics and Mathematics of the Universe (Kavli IPMU), the University of Tokyo, the High Energy Accelerator Research Organization (KEK), the Academia Sinica Institute for Astronomy and Astrophysics in Taiwan (ASIAA), and Princeton University. Funding was contributed by the FIRST program from the Japanese Cabinet Office, the Ministry of Education, Culture, Sports, Science and Technology (MEXT), the Japan Society for the Promotion of Science (JSPS), Japan Science and Technology Agency (JST), the Toray Science Foundation, NAOJ, Kavli IPMU, KEK, ASIAA, and Princeton University.

This paper makes use of software developed for the Large Synoptic Survey Telescope (LSST; Jurić et al. 2017; Ivezić et al. 2019). We thank the LSST Project for making their code available as free software at <http://dm.lsst.org>.

This paper is based in part on data collected at the Subaru Telescope and retrieved from the HSC data archive system, which is operated by Subaru Telescope and Astronomy Data Center (ADC) at NAOJ. Data analysis was in part carried out

with the cooperation of Center for Computational Astrophysics (CfCA), NAOJ.

The Pan-STARRS1 Surveys (PS1; Schlafly et al. 2012; Tonry et al. 2012; Magnier et al. 2013; Chambers et al. 2016) and the PS1 public science archive have been made possible through contributions by the Institute for Astronomy, the University of Hawaii, the Pan-STARRS Project Office, the Max Planck Society and its participating institutes, the Max Planck Institute for Astronomy, Heidelberg, and the Max Planck Institute for Extraterrestrial Physics, Garching, The Johns Hopkins University, Durham University, the University of Edinburgh, the Queens University Belfast, the Harvard-Smithsonian Center for Astrophysics, the Las Cumbres Observatory Global Telescope Network Incorporated, the National Central University of Taiwan, the Space Telescope Science Institute, the National Aeronautics and Space Administration under grant No. NNX08AR22G issued through the Planetary Science Division of the NASA Science Mission Directorate, the National Science Foundation grant No. AST-1238877, the University of Maryland, Eotvos Lorand University (ELTE), the Los Alamos National Laboratory, and the Gordon and Betty Moore Foundation.

This study is based on observations obtained at the Gemini Observatory via the time exchange program between Gemini and the Subaru Telescope, processed using the Gemini IRAF package. The Gemini Observatory is operated by the Association of Universities for Research in Astronomy, Inc., under a cooperative agreement with the NSF on behalf of the Gemini partnership: the National Science Foundation (United States), National Research Council (Canada), CONICYT (Chile), Ministerio de Ciencia, Tecnología e Innovación Productiva (Argentina), Ministério da Ciência, Tecnologia e Inovação (Brazil), and Korea Astronomy and Space Science Institute (Republic of Korea).

The National Radio Astronomy Observatory is a facility of the National Science Foundation operated under cooperative agreement by Associated Universities, Inc.

GMRT is run by the National Centre for Radio Astrophysics of the Tata Institute of Fundamental Research.

This research has made use of the Vizier catalog access tool, CDS, Strasbourg, France.

This work is financially supported by the Japan Society for the Promotion of Science (JSPS) KAKENHI grants: Nos. 16H01101 (T.N.), 16H03958 (T.N.), 17H01114 (T.N. & Y.O.), 17H04830 (Y.M.), 17H06130 (K.K.), 18K13584 (K.I.), 18J01050 (Y.T.), 19K14759 (Y.T.), and JP20K14529 (T.K.). Y.M. acknowledges the support from the Mitsubishi Foundation grant No. 30140. K.K. acknowledges the support from the NAOJ ALMA Scientific Research Grant Number 2017-06B.

*Facilities:* Subaru (HSC), Gemini:South (GMOS), VLA, GMRT.

*Software:* Python, astropy, Gemini IRAF, CIGALE.

## ORCID iDs

Takuji Yamashita <https://orcid.org/0000-0002-4999-9965>  
 Tohru Nagao <https://orcid.org/0000-0002-7402-5441>  
 Hiroyuki Ikeda <https://orcid.org/0000-0002-1207-1979>  
 Yoshiaki Toba <https://orcid.org/0000-0002-3531-7863>  
 Masaru Kajisawa <https://orcid.org/0000-0002-1732-6387>  
 Masayuki Tanaka <https://orcid.org/0000-0002-5011-5178>  
 Masayuki Akiyama <https://orcid.org/0000-0002-2651-1701>  
 Yuichi Harikane <https://orcid.org/0000-0002-6047-430X>

Kohei Ichikawa <https://orcid.org/0000-0002-4377-903X>  
 Taiki Kawamuro <https://orcid.org/0000-0002-6808-2052>  
 Kotaro Kohno <https://orcid.org/0000-0002-4052-2394>  
 Chien-Hsiu Lee <https://orcid.org/0000-0003-1700-5740>  
 Kianhong Lee <https://orcid.org/0000-0003-4814-0101>  
 Masafusa Onoue <https://orcid.org/0000-0003-2984-6803>

## References

- Abazajian, K., Adelman-McCarthy, J. K., Agüeros, M. A., et al. 2004, *AJ*, **128**, 502
- Aihara, H., Arimoto, N., Armstrong, R., et al. 2018a, *PASJ*, **70**, S4
- Aihara, H., Armstrong, R., Bickerton, S., et al. 2018b, *PASJ*, **70**, S8
- Akiyama, M., He, W., Ikeda, H., et al. 2018, *PASJ*, **70**, S34
- Ando, M., Ohta, K., Iwata, I., et al. 2006, *ApJL*, **645**, L9
- Bañados, E., Venemans, B. P., Morganson, E., et al. 2015, *ApJ*, **804**, 118
- Becker, R. H., White, R. L., & Helfand, D. J. 1995, *ApJ*, **450**, 559
- Boquien, M., Burgarella, D., Roehly, Y., et al. 2019, *A&A*, **622**, A103
- Bosch, J., Armstrong, R., Bickerton, S., et al. 2018, *PASJ*, **70**, S5
- Bruzual, G., & Charlot, S. 2003, *MNRAS*, **344**, 1000
- Burgarella, D., Buat, V., & Iglesias-Páramo, J. 2005, *MNRAS*, **360**, 1413
- Calzetti, D., Armus, L., Bohlin, R. C., et al. 2000, *ApJ*, **533**, 682
- Carilli, C. L., & Yun, M. S. 1999, *ApJL*, **513**, L13
- Chabrier, G. 2003, *PASP*, **115**, 763
- Chambers, K. C., Magnier, E. A., Metcalfe, N., et al. 2016, arXiv:1612.05560
- Condon, J. J., Cotton, W. D., Greisen, E. W., et al. 1998, *AJ*, **115**, 1693
- Croton, D. J., Springel, V., White, S. D. M., et al. 2006, *MNRAS*, **365**, 11
- Cutri, R. M., et al. 2014, *yCat*, **2328**, 0
- De Breuck, C., Bertoldi, F., Carilli, C., et al. 2004, *A&A*, **424**, 1
- De Breuck, C., Röttgering, H., Miley, G., van Breugel, W., & Best, P. 2000a, *A&A*, **362**, 519
- De Breuck, C., Seymour, N., Stern, D., et al. 2010, *ApJ*, **725**, 36
- De Breuck, C., van Breugel, W., Röttgering, H. J. A., & Miley, G. 2000b, *A&AS*, **143**, 303
- de Gasperin, F., Intema, H. T., & Frail, D. A. 2018, *MNRAS*, **474**, 5008
- Douglas, J. N., Bash, F. N., Bozyan, F. A., et al. 1996, *AJ*, **111**, 1945
- Dunlop, J. S., & Peacock, J. A. 1990, *MNRAS*, **247**, 19
- Edge, A., Sutherland, W., Kuijken, K., et al. 2013, *Msngr*, **154**, 32
- Fabian, A. C. 2012, *ARA&A*, **50**, 455
- Falkendal, T., De Breuck, C., Lehnert, M. D., et al. 2019, *A&A*, **621**, A27
- Furusawa, H., Koike, M., Takata, T., et al. 2018, *PASJ*, **70**, S3
- Harikane, Y., Ouchi, M., Ono, Y., et al. 2018, *PASJ*, **70**, S11
- Helfand, D. J., White, R. L., & Becker, R. H. 2015, *ApJ*, **801**, 26
- Ichikawa, K., Yamashita, T., & Toba, Y. 2020, *ApJ*, submitted
- Intema, H. T., Jagannathan, P., Mooley, K. P., & Frail, D. A. 2017, *A&A*, **598**, A78
- Ivezić, Ž., Kahn, S. M., Tyson, J. A., et al. 2019, *ApJ*, **873**, 111
- Jarvis, M. J., & Rawlings, S. 2000, *MNRAS*, **319**, 121
- Jarvis, M. J., Rawlings, S., Willott, C. J., et al. 2001, *MNRAS*, **327**, 907
- Jarvis, M. J., Teimourian, H., Simpson, C., et al. 2009, *MNRAS*, **398**, L83
- Jurić, M., Kantor, J., Lim, K.-T., et al. 2017, in ASP. Conf. Ser. 512, *Astronomical Data Analysis Software and Systems XXV*, ed. N. P. F. Lorente, K. Shorridge, & R. Wayth (San Francisco, CA: ASP), 279
- Kawanomoto, S., Uruguchi, F., Komiyama, Y., et al. 2018, *PASJ*, **70**, 66
- Klamer, I. J., Ekers, R. D., Bryant, J. J., et al. 2006, *MNRAS*, **371**, 852
- Komiyama, Y., Obuchi, Y., Nakaya, H., et al. 2018, *PASJ*, **70**, S2
- Kopylov, A. I., Goss, W. M., Pariškiš, Y. N., et al. 2006, *AsTL*, **32**, 433
- Madau, P. 1995, *ApJ*, **441**, 18
- Magnier, E. A., Schlafly, E., Finkbeiner, D., et al. 2013, *ApJS*, **205**, 20
- Matsuoka, K., Nagao, T., Maiolino, R., et al. 2009, *A&A*, **503**, 721
- Matsuoka, Y., Iwasawa, K., Onoue, M., et al. 2018a, *ApJS*, **237**, 5
- Matsuoka, Y., Onoue, M., Kashikawa, N., et al. 2016, *ApJ*, **828**, 26
- Matsuoka, Y., Onoue, M., Kashikawa, N., et al. 2018b, *PASJ*, **70**, S35
- Matsuoka, Y., Onoue, M., Kashikawa, N., et al. 2019, *ApJL*, **872**, L2
- Mauch, T., Klöckner, H.-R., Rawlings, S., et al. 2013, *MNRAS*, **435**, 650
- McNamara, B. R., Nulsen, P. E. J., Wise, M. W., et al. 2005, *Natur*, **433**, 45
- Miley, G., & De Breuck, C. 2008, *A&ARv*, **15**, 67
- Miyazaki, S., Komiyama, Y., Kawanomoto, S., et al. 2018, *PASJ*, **70**, S1
- Morabito, L. K., & Harwood, J. J. 2018, *MNRAS*, **480**, 2726
- Morganti, R., Fogasy, J., Paragi, Z., Oosterloo, T., & Orienti, M. 2013, *Sci*, **341**, 1082
- Nagao, T., Maiolino, R., & Marconi, A. 2006, *A&A*, **447**, 863
- Oke, J. B., & Gunn, J. E. 1983, *ApJ*, **266**, 713
- Ono, Y., Ouchi, M., Harikane, Y., et al. 2018, *PASJ*, **70**, S10
- Overzier, R. A., Miley, G. K., Bouwens, R. J., et al. 2006, *ApJ*, **637**, 58

- Pérez-González, P. G., Rieke, G. H., Villar, V., et al. 2008, *ApJ*, 675, 234
- Rengelink, R. B., Tang, Y., de Bruyn, A. G., et al. 1997, *A&AS*, 124, 259
- Reuland, M., Röttgering, H., van Breugel, W., & De Breuck, C. 2004, *MNRAS*, 353, 377
- Rigby, E. E., Argyle, J., Best, P. N., Rosario, D., & Röttgering, H. J. A. 2015, *A&A*, 581, A96
- Rocca-Volmerange, B., Le Borgne, D., De Breuck, C., Fioc, M., & Moy, E. 2004, *A&A*, 415, 931
- Roettgering, H. J. A., van Ojik, R., Miley, G. K., et al. 1997, *A&A*, 326, 505
- Saxena, A., Jagannathan, P., Röttgering, H. J. A., et al. 2018a, *MNRAS*, 475, 5041
- Saxena, A., Marinello, M., Overzier, R. A., et al. 2018b, *MNRAS*, 480, 2733
- Saxena, A., Röttgering, H. J. A., Duncan, K. J., et al. 2019, *MNRAS*, 489, 5053
- Schlafly, E. F., Finkbeiner, D. P., Jurić, M., et al. 2012, *ApJ*, 756, 158
- Schlegel, D. J., Finkbeiner, D. P., & Davis, M. 1998, *ApJ*, 500, 525
- Seymour, N., Stern, D., De Breuck, C., et al. 2007, *ApJS*, 171, 353
- Spinrad, H., Djorgovski, S., Marr, J., et al. 1985, *PASP*, 97, 932
- Steidel, C. C., Giavalisco, M., Pettini, M., Dickinson, M., & Adelberger, K. L. 1996, *ApJL*, 462, L17
- Tanaka, M. 2015, *ApJ*, 801, 20
- Toba, Y., Yamashita, T., Nagao, T., et al. 2019, *ApJS*, 243, 15
- Tonry, J. L., Stubbs, C. W., Lykke, K. R., et al. 2012, *ApJ*, 750, 99
- Toshikawa, J., Uchiyama, H., Kashikawa, N., et al. 2018, *PASJ*, 70, S12
- van Breugel, W., De Breuck, C., Stanford, S. A., et al. 1999, *ApJL*, 518, L61
- Waddington, I., Windhorst, R. A., Cohen, S. H., et al. 1999, *ApJL*, 526, L77
- Wagner, A. Y., & Bicknell, G. V. 2011, *ApJ*, 728, 29
- Yabe, K., Ohta, K., Iwata, I., et al. 2009, *ApJ*, 693, 507
- Yamashita, T., Nagao, T., Akiyama, M., et al. 2018, *ApJ*, 866, 140
- York, D. G., Adelman, J., Anderson, J. E., Jr., et al. 2000, *AJ*, 120, 1579
- Yuan, Z., Wang, J., Zhou, M., & Mao, J. 2016, *ApJ*, 829, 95
- Yuan, Z., Wang, J., Zhou, M., Qin, L., & Mao, J. 2017, *ApJ*, 846, 78